Solution Structure and Dynamics of a Complex between DNA and the Antitumor Bisnaphthalimide LU-79553: Intercalated Ring Flipping on the Millisecond Time Scale[†,‡]

José Gallego* and Brian R. Reid

Chemistry Department, University of Washington, Seattle, Washington 98195-1700

Received July 9, 1999; Revised Manuscript Received September 3, 1999

ABSTRACT: Using a combination of nuclear magnetic resonance (NMR) spectroscopy experiments and molecular dynamics, we have analyzed the structure and dynamics of a complex between the bisnaphthalimide drug LU-79553 and the DNA duplex d(ATGCAT)$_2$. LU-79553 is a DNA-binding topoisomerase II inhibitor that is particularly effective against human solid tumors that are refractory to other drugs. We have found that the two naphthalimide chromophores of the drug bisintercalate at the TpG and CpA steps of the DNA hexanucleotide, stacking mainly with the purine G and A bases from opposite strands. The 3,7-diazanonylene linker lies in the major groove of the DNA molecule, with its two amino groups hydrogen-bonded to the symmetry-related guanine bases. Unexpectedly, we have detected an unprecedented exchange process between two equivalent and intercalated states of the naphthalimide rings in the drug−DNA complex. The interconversion process takes place by rotational ring flipping, has an activation energy of 22 kcal mol^{-1} for the two rings, and does not affect the aminoalkyl linker region of the drug. The exchange rate is intermediate to fast on the chemical shift time scale at 36 °C (1800 s^{-1}) but slow at 2 °C (20 s^{-1}). We have also observed limited flexibility for the drug linker on the picosecond time scale on the basis of NMR data and a time-averaged restrained molecular dynamics simulation. The implications of the structural and dynamic features of the DNA−LU-79553 complex on the binding specificity and on the antitumor activity of bisnaphthalimide agents are discussed.

Bisnaphthalimide agents are active against human solid tumors that are refractory to many other anticancer drugs (*1*). These compounds are dimeric derivatives of the monointercalating drugs amonafide and mitonafide. They bind to DNA as bisintercalators (*2*) and show higher binding affinity and greater cytotoxic activity than their parent monointercalators (*3*). In particular, the bisnaphthalimide LU-79553 (Figure 1a) exhibits excellent activity against human xenograft tumors in mice and has been selected for clinical development (*4*). The closely related agent DMP-840 (also called bisnafide) is now in phase II clinical trials, where it is being tested in patients with refractory solid tumors (*5*). Given the pharmacological potential of these agents, new naphthalimides combined with nitrogen mustard and lexitropsin moieties are under investigation as DNA-directed drugs (*6*), and a chemically related naphthalenediimide derivative has been recently reported to be a DNA tetraintercalator by Lokey et al. (*7*).

There is evidence that naphthalimide agents inhibit the activity of topoisomerase II (*1*, *3*, *8*, *9*). Since the pharmacophore of many topoisomerase-interfering compounds contains a DNA-binding portion (*10*), the characterization of their interactions with DNA will shed light on their mechanism of cytotoxicity.

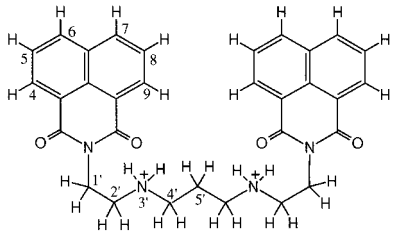

FIGURE 1: (a) Chemical structure of LU-79553 (LU) with its atom numbering scheme. (b) The d(ATGCAT)$_2$ duplex (D6) with its residue numbering scheme and with the LU bisintercalation site shown schematically.

Viscosimetry studies by Bailly et al. (*2*) have shown that LU-79553 and related analogues bisintercalate into DNA. Using footprinting experiments and chemical probing, these researchers concluded that the interaction is sequence-specific and takes place from the major groove; a preference for mixed purine−pyrimidine dinucleotide steps at the drug

[†] This work was supported by a fellowship from Fundación Ramón Areces (Spain) to J.G. and by NIH Grants GM-32681 and GM-52883 to B.R.R.

[‡] The coordinates of the d(ATGCAT)$_2$−LU-79553 refined structures have been deposited in the Brookhaven Protein Data Bank (PDB ID 1CX3).

* Corresponding author: e-mail jgallego@u.washington.edu; fax 1-206-685-8665.

10.1021/bi9915869 CCC: $18.00
Published on Web 10/29/1999

binding sites was also reported. However, it was not established exactly where in the target sequence the naphthalimides intercalate, and no NMR[1] or X-ray structures of a naphthalimide or a bisnaphthalimide complexed with DNA have been published to date.

In this study we analyze, using a combination of NMR spectroscopy experiments and molecular dynamics, the structure and dynamics of a complex between the bisnaphthalimide agent LU-79553 (designated LU) and the DNA duplex d(ATGCAT)$_2$ (hereafter referred to as D6) (Figure 1). We show that the two naphthalimide chromophores of LU sandwich the central GpC step of the hexanucleotide, intercalating at the symmetrical TpG (CpA) steps. The aminoalkyl linker lies in the major groove of the DNA molecule, with its amino groups hydrogen-bonded to the two symmetry-related guanine bases. We have detected limited flexibility for the LU linker on the picosecond time scale and, surprisingly, a rotational flipping of the intercalated naphthalimide chromophores. This last process occurs at a rate of 20 s^{-1} at 2 °C and does not affect the aminoalkyl linker portion of the drug.

MATERIALS AND METHODS

Sample Preparation. The bisnaphthalimide LU-79553 [bismethanesulfonate salt] was provided by Knoll AG. d(ATGCAT) was synthesized on an Applied Biosystems 394 DNA synthesizer, and purified as described elsewhere (*11*). Purified oligonucleotide (0.9 μmol, 1.6 mg) was dissolved in an aqueous buffer consisting of 20.0 mM sodium phosphate (pH 7.2) and 0.2 mM EDTA, yielding a concentration of 2.0 mM (DNA strand) in 0.45 mL. The 1:1 drug−duplex complex was formed by progressively adding microliter aliquots of a 25 mM stock solution of LU in ^2H_2O and monitoring the titration by 1D NMR. The concentrations of DNA and drug were calculated by using a nearest-neighbor model for D6 (*12*) and an extinction coefficient of 45 623 M^{-1} cm^{-1} (at 232 nm) for LU, respectively.

NMR Spectroscopy. The NMR experiments were carried out on Bruker DRX-500 and DMX-750 NMR spectrometers. The data were processed on SG INDIGO2 workstations with FELIX 95.0 software (BIOSYM Inc.). For experiments in ^1H_2O, the water signal was suppressed with a jump-and-return sequence with gradients (*13*). NOESY experiments were carried out in the phase-sensitive TPPI mode, collecting 2048 points in t_2 and 800 experiments in t_1 and averaging either 48 or 32 scans per t_1 incrementation. DNA−naphthalimide intermolecular NOEs mediated by chemical exchange were identified by performing a series of NOESY experiments in which each of the LU aromatic resonances was selectively irradiated during the 50 ms mixing period (*14*). All NOESY data were apodized by use of a 90°-shifted sine bell-squared function in both dimensions. DQF−COSY, ROESY, TOCSY (mixing times 30 and 80 ms), and pure chemical exchange (*15*) spectra were also collected in the phase-sensitive TPPI mode with 2048 and 800 points in t_2 and t_1, respectively, and 32 scans for each t_1 experiment. The pure chemical exchange spectra were acquired by interleaving a series of NOESY and ROESY periods during the mixing time in order to eliminate dipolar cross-relaxation (*15*). The COSY data were processed with 6 Hz of Gaussian line narrowing in t_2 and a 45°-shifted sine bell function in t_1; the TOCSY, ROESY, and NOESY−ROESY data were processed as explained for NOESY experiments. A proton-detected $^{31}P-^1H$ heteronuclear correlation spectrum (*16*) was also collected in the hypercomplex mode, with 2048 points in the t_2 (^1H) dimension and 100 complex points in the t_1 (^{31}P) dimension, and 256 scans for each t_1 incrementation. The $^{31}P-^1H$ data were apodized with a 6 Hz Gaussian line-narrowing window function in the t_2 dimension and a 45°-shifted sine bell function in the t_1 dimension. The relaxation delay was either 2 or 4 s for all of the above experiments. Spin−lattice relaxation times (T_1) for drug and DNA protons were obtained by the inversion recovery method, with 30 partial recovery periods and a 20 s recycle delay. Except where indicated, all experiments were carried out at 2 °C, where sufficiently narrow drug line widths together with minimal peak overlap were observed (Figure 2).

Naphthalimide Ring Exchange Rates. The flipping rate constant of the LU naphthalimide chromophores at various low temperatures was obtained from the rate of magnetization transfer between the resolved H4 and H9 naphthalimide protons, which are more than 6.5 Å apart (Figure 1a). The z magnetization (M) of the H9 proton was measured as a function of the time (t) during which H4 was selectively irradiated with a weak RF field. A series of difference spectra were obtained by subtraction of reference spectra acquired with equivalent contralateral irradiation. The resulting experimental curves were fit to the theoretical expression (*17*):

$$M(t) = M_0[\tau_1/\tau \exp(-t/\tau_1) + \tau_1/T_1]$$

where M_0 is the equilibrium longitudinal magnetization of H9. The interconversion rate constant k was obtained from the exponential decay constant $1/\tau_1$ (Figure 8a), using $k = 1/\tau = 1/\tau_1 - 1/T_1$. In our case, $1/T_1$ is much smaller than $1/\tau_1$, and T_1 was obtained from inversion recovery experiments. The rate constants obtained by this method are within 2 s^{-1} from the corresponding values obtained from the initial build-up (*18*) of the H4−H9 NOESY cross-peak at two different temperatures. At higher temperatures (≥6 °C), the rate constants were calculated with the lineshape analysis program MEXICO (*19*). The scalar coupling constants of the naphthalimide system were included in the calculations, and the line width of G3 H8, not affected by exchange, was used as a reference. The Arrhenius activation energy (E_a) for the LU two-ring flipping motion was obtained by fitting the experimental data to the expression $k(T) = A \exp(-E_a/RT)$ (Figure 8b).

Order Parameters. In the model-free formalism of Lipari and Szabo (*20*), the order parameter S^2 measures the orientational freedom of an internuclear vector **r** within a tumbling molecule. If the internal motion of **r** is fast with respect to the overall tumbling rate

$$S^2 = \sigma r^6/\sigma_r r_r^6$$

[1] Abbreviations: EDTA, ethylenediaminetetraacetic acid; D6, d(ATGCAT)$_2$; DQF, double quantum filtered; COSY, correlation spectroscopy; LU, LU-79553; MD, molecular dynamics; ppm, parts per million; NMR, nuclear magnetic resonance; NOE, nuclear Overhauser effect; NOESY, nuclear Overhauser effect spectroscopy; PME, particle mesh Ewald; r-MD, restrained molecular dynamics; rms, root-mean-square; ROESY, rotating frame Overhauser effect spectroscopy; tar-MD, time-averaged restrained molecular dynamics; TOCSY, total correlation spectroscopy; TPPI, time-proportional phase incrementation.

after $S_r^2 = 1$ is assigned for a reference interproton vector, in our case C4 H5−H6 ($r_r = 2.46$ Å). We used $r = 1.78$ Å for DNA and LU methylene proton pairs. The cross-relaxation rate constants σ and σ_r were measured by fitting NOESY cross-peak intensities obtained at short mixing times (Table 2) and scaled by diagonal intensities (*21*).

Structure Determination and Refinement. Distances between nonexchangeable protons were initially given bounds of 2.0−3.5, 3.5−4.5, or 4.5−5.5 Å based on the build-up rate of NOESY cross-peaks integrated at 50, 100, 150, and 200 ms mixing times, and using the C4 H5−H6 cross-peak as the reference distance. The corresponding NOESY spectra were collected without interruption at 750 MHz with 48 scans and a 4-s relaxation delay. For methyl protons, the distances from a methyl pseudoatom were similarly scaled by using the thymine H6−CH_3 cross-peaks ($r = 2.9$ Å). Distances involving exchangeable protons were set with generous bounds upon visual inspection of the intensities of the corresponding ^1H_2O NOESY cross-peaks at 50, 100, and 150 ms mixing times. An additional set of hydrogen-bonding distance restraints was used to maintain base pairing in the double helix, since convincing evidence for these hydrogen bonds was observed (see Results). The D6 backbone dihedrals were conservatively constrained to 0° ± 150° (for α and ζ), 180° ± 60/80° (for β), 60° ± 60° (for γ), and 180° ± 60° or 240° ± 140° (for ϵ), based on the analysis of P−H4′/H2′ cross-peaks, ^{31}P chemical shifts (*22*), H2′-H5′/H5″ and H6/H8−H5′/H5″ NOEs, H5′/H5″ line widths, and ΣJ measurements for H3′ and H4′ resonances (*23*) in both D6 and D6−LU. Chirality constraints were imposed on asymmetric sugar carbons as appropriate.

By use of distance geometry, 20 structures were embedded in three-dimensional space from the bounds matrix and subsequently minimized. The structures were then subjected to 20 ps of restrained molecular dynamics (r-MD) using AMBER (*24, 25*), with specific covalent parameters and ab initio 6-31G* atomic charges for LU (Gallego et al., unpublished results). The systems were quickly heated to 900 K in 2 ps, kept at that temperature for 4 ps, slowly cooled to 9 K in the remaining 14 ps, and subsequently minimized. The force constants for the distance and dihedral restraint terms (30 kcal mol^{-1} Å^{-2} and 90 kcal mol^{-1} rad^{-2}, respectively) were progressively decreased to 10% of their initial values during the heating period and increased back to their full values during the cooling period. We used a time step of 1.0 fs, a distance-dependent dielectric constant of $4r_{ij}$, and no cutoff distance for the nonbonded interactions.

The time-dependent NOESY spectra of the structure with the lowest total and restraint energies were subsequently back-calculated with an improved version of BIRDER (*26*) incorporating a three-jump rotational model for the methyl groups. Intermolecular NOEs between LU and D6 were not refined and were assigned generous bounds, since evidence of internal LU motion was detected (see Results). LU linker methylene proton pairs were treated as pseudoatoms. An isotropic tumbling time of 2.5 ns, obtained from the C4 H5−H6 cross-relaxation rate, was used. Distance constraints were then adjusted, on the basis of a comparison of the calculated and experimental NOE intensities in all spectral regions at 50, 100, 150, and 200 ms mixing times. To account for volume integration uncertainties, 10% distance error bounds were superimposed over the smaller bounds due to 2D baseline noise. This distance geometry/r-MD/relaxation matrix simulation refinement procedure was repeated until there were no significant improvements in the simulated NOESY spectra. Distance constraints for overlapped cross-peaks as well as repulsive constraints were added during the iterative refinement rounds. At the final stage of the refinement, 15 out of 20 structures converged to similar values of potential energy and restraint energy terms and were selected for the analyses. The final NOE R factors were calculated from 58 cross-peaks at four mixing times (232 intensities) as $R = (1/N) \sum |I_c - I_e|/I_e$, where I_e and I_c are the experimental and calculated N NOE intensities, respectively.

Time-Averaged Restrained Molecular Dynamics. Eight Na^+ counterions were placed on the OPO bisectors (except P3 in both strands) of one of the 15 refined D6−LU structures, and the resulting neutral system was immersed in a rectangular box of 2250 TIP3P water molecules, upon which periodic boundary conditions were applied. For this solvated system, the force field of Cornell et al. (*27*) was used in subsequent calculations with AMBER 5.0. Water molecules and counterions were progressively equilibrated by a combination of 3000 cycles of energy minimization and 22 ps of r-MD, during which the D6 and LU atoms were restrained to their initial positions with a harmonic potential of 25 kcal mol^{-1} Å^{-2}. This last term was then turned off, and 20 ps of r-MD was carried out in four stages at 100, 200, 250, and 300 K. This was followed by the final 400 ps tar-MD production period at 300 K and 1 atm, during which the interproton and hydrogen-bonding restraints were time-averaged (*28*) with an exponential decay constant of 20 ps and a pseudoforce constant of 1 kcal mol^{-1} Å^{-2}. No dihedral or chiral constraints were imposed during the tar-MD stage. System coordinates were saved every 1 ps. Throughout the calculations, we used a dielectric constant of 1 and a residue-based cutoff distance of 9 Å for the nonbonded interactions, a time step of 2 fs, and heat and pressure bath coupling constants of 0.5 ps. Electrostatic interactions were computed with the particle mesh Ewald (PME) method (*29*), using a grid spacing of approximately 1 Å and a direct sum tolerance of 10^{-5}. The monitored rms deviation of the D6−LU coordinates with respect to the initial structure (1.14 ± 0.18 Å) indicated an equilibrated system throughout the tar-MD trajectory.

Analysis. Structural analyses on the 15 back-calculated and 400 tar-MD D6−LU structures were carried out with NEWHELIX (*30*), RNA (*31*) and a variety of FORTRAN programs written by J.G.

RESULTS

Sequence-Specific Binding of LU-79553 to d(ATGCAT)$_2$. The ^{1}H NMR spectra of the D6−LU 1:1 complex at 2 °C are shown in Figure 2. The presence of a single set of modified D6 and LU resonances in the 1:1 D6−LU mixture indicates that a unique drug−DNA complex is formed in solution that retains the 2-fold symmetry observed for both the isolated LU and the palindromic DNA molecule. This also indicates stable binding of the drug to a specific binding site in the double-helical DNA receptor. We will later demonstrate, however, that at 2 °C the LU naphthalimide rings are in fact exchanging (flipping) slowly on the chemical shift time scale between two equivalent *intercalated* states.

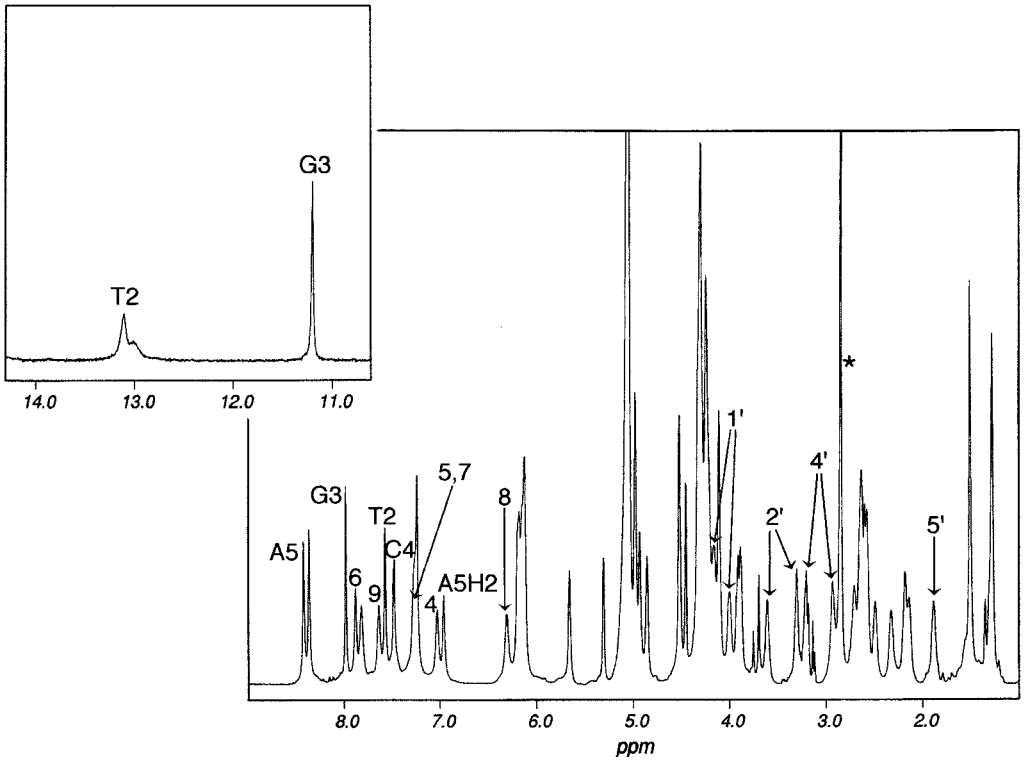

FIGURE 2: $^{2}H_2O$ ^{1}H NMR spectra of the 1:1 D6−LU complex (750 MHz) at 2 °C. The inset shows the imino proton region of the corresponding $^{1}H_2O/^{2}H_2O$ spectra. The nonterminal aromatic D6 assignments and the LU assignments (atom numbers) are labeled over the resonances. The NMR line of the LU methanesulfonate counterion is labeled with an asterisk.

DNA Assignments and NOE Interactions. All proton and phosphorus resonances in D6 and in the D6−LU complex have been assigned (Supporting Information) from NOESY connectivities combined with COSY, TOCSY, and $^{1}H-^{31}P$ correlation data.

The imino protons of both D6 and D6−LU resonate in the 12 to 14 ppm spectral region, with the exception of G3 HN1 in the complex, which is shifted upfield to 11.2 ppm (Figure 2). The detectable G3, C4, and A5 hydrogen-bonded and external (nonbonded) amino proton resonances in both the free and bound D6 are well separated. This indicates base pairing in both D6 alone and the D6−LU complex, as is also confirmed by the T2 HN3−A5 H2 and G3 HN1−C4 HN4 NOEs observed at 2 °C in both species (not shown).

The D6 protons most affected by LU binding are the above-mentioned G3 HN1 as well as the C4 HN4 (internal), A5 H2, and T2 HN3 protons, which undergo upfield shifts of 1.6, 1.1, 0.9, and 0.7 ppm, respectively (Figure 2). These upfield shifts, induced by the ring-current effects of the naphthalimide rings, are characteristic of intercalative binding to DNA and provide information on the regions of the DNA molecule most closely bound by LU (see below).

Standard sequential and intrasugar NOESY and COSY interactions indicate that D6 alone forms a B-type double helix in solution. The D6−LU complex retains the 2-fold symmetry of free D6, but the H6/H8−H1′/H2′ NOE connectivity pathways typical of right-handed DNA duplexes are weaker at the T2pG3 and C4pA5 steps in the complex (Figure 3). This indicates that the LU rings bisintercalate at these positions in the DNA duplex (Figure 1b), pushing the T2:A5 and G3:C4 base pairs apart and thus increasing the corresponding sequential base−sugar interproton distances.

The glycosidic torsion angles of all nucleotides in the D6−LU complex are in the anti range, as established by the intensities of the intraresidue H8/H6−H1′ NOEs (Figure 3b). The intensity patterns of the D6−LU intrasugar H1′/H3′−H2′/H2″ and H3′−H4′ COSY cross-peaks, as well as the intraresidue H6/H8−H2′/H2″/H3′ and intrasugar H1′/H2″−H4′ NOEs, indicate S-type sugar conformations (pseudorotation phase angle $P > 100°$) for G3 and A5 but unusual conformations for the T2 and C4 sugars, located 5′ to the intercalated LU rings.

LU Assignments and NOE Interactions. Upon binding to D6, all of the drug protons except for the linker H5′1/2 pair (Figure 1a) lose the degeneracy observed in the NMR spectrum of free LU and split into two resonances in the D6−LU complex (Figure 2) due to different binding environments. The assignments of the naphthalimide and aminoalkyl linker protons were obtained from COSY spectra combined with 30 and 80 ms TOCSY spectra. The naphthalimide "central" positions H5 and H8 (see Figure 1a) were easily identified because they give rise to two COSY cross-peaks with their vicinal, "internal" protons (H6 or H7) and the more peripheral, "external" protons (H4 or H9) in each benzene ring (Figure 1a).

Unexpectedly, we also found that in NOESY experiments at very short mixing times, each LU naphthalimide proton in D6−LU is connected with its symmetrical counterpart by a very intense cross-peak (i.e., H4, H5, and H6 exhibit strong cross-peaks to H9, H8, and H7, respectively). Since the H4−H9 and H5−H8 pairs are more than 6.5 Å apart (Figure 1a), such cross-peaks cannot be caused by dipolar relaxation and must therefore be due to conformational exchange. ROESY spectra as well as pure chemical exchange experiments (*15*) confirmed this conclusion, showing strong cross-peaks

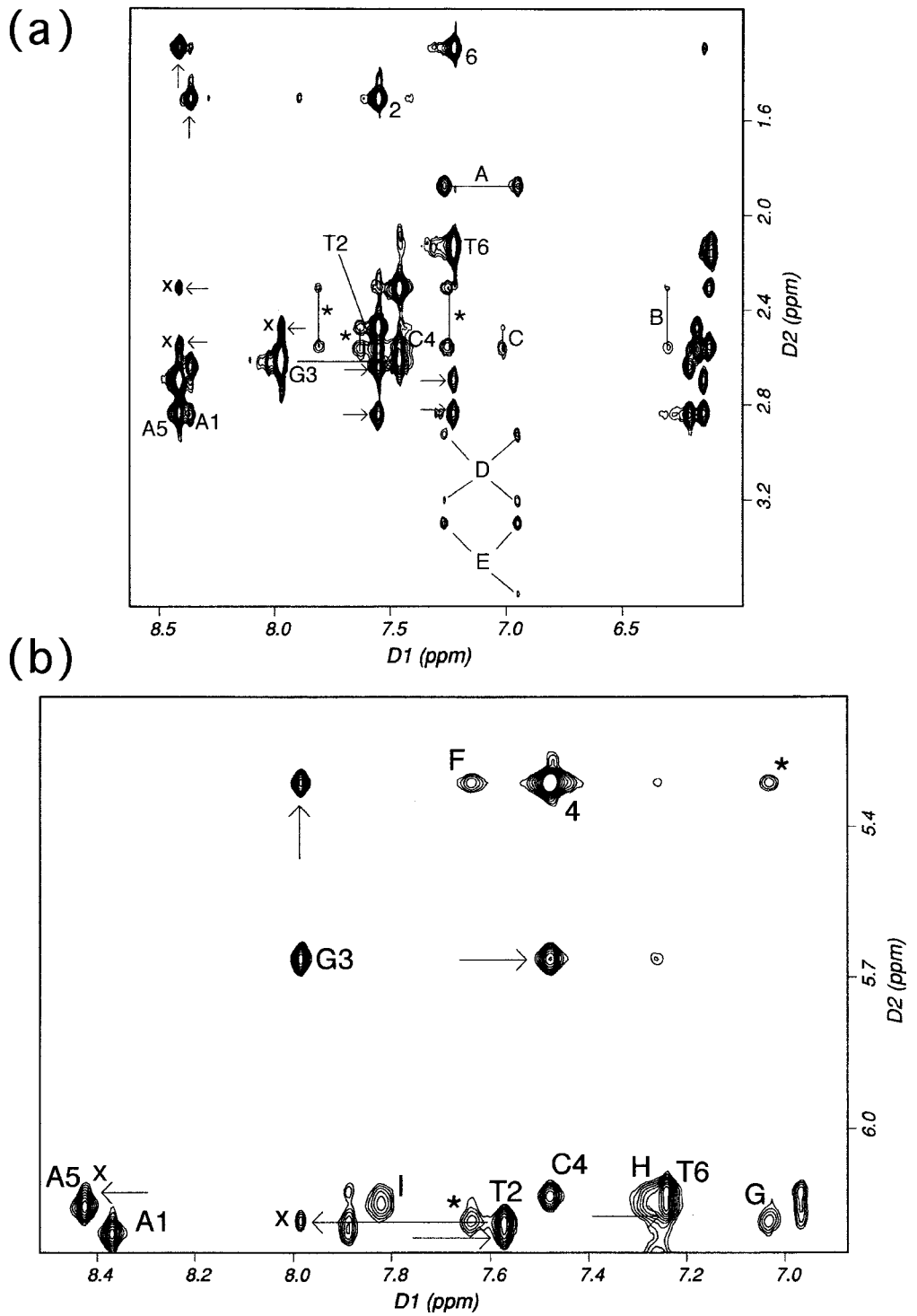

FIGURE 3: (a) NOESY contour plot (750 MHz, 150 ms mixing time) of the D6−LU complex in $^1H_2O/^2H_2O$ at 2 °C, showing the NOE connectivities between the aromatic and high-field regions of the spectrum. (Note: Cross-peaks closer to the residual ^1H_2O resonance at 5.1 ppm are less intense due to solvent suppression.) (b) Assignment of the aromatic and H1′ region of the 750 MHz NOESY spectrum (150 ms) of D6−LU in ^2H_2O at 2 °C. In both panels, the intraresidue H6/H8−H1′ and H6/H8−H2″ cross-peaks are labeled with the corresponding residue name and number. The intraresidue thymine H6−CH_3 and cytosine H6−H5 cross-peaks are designated with their residue number. The sequential (*n*) H1′/H2′/H2″−(*n* + 1) H6/H8 NOEs are connected to the corresponding intraresidue (*n*) H6/H8−H1′/H2′/H2″ cross-peaks with horizontal arrows. These connectivities are weaker for the T2pG3 and C4pA5 steps (marked with x) due to LU bisintercalation. LU-D6 NOEs mediated by chemical exchange are labeled with asterisks. Intermolecular LU-D6 cross-peaks A to I are assigned as follows (hb, hydrogen-bonded; e, exposed): A, C4 HN4(hb)−LU H5′1/2, C4 HN4(e)−LU H5′1/2; B, C4 H2′−LU H8, C4 H2″−LU H8; C, T2 H2′−LU H4, T2 H2″−LU H4; D, C4 HN4(hb)−LU H4′1, C4 HN4(hb)−LU H4′2, C4 HN4(e)−LU H4′1, C4 HN4(e)−LU H4′2; E, C4 HN4(hb)−LU H2′1, C4 HN4(e)−LU H2′1, C4 HN4(e)−LU H2′2; F, C4 H5−LU H9; G, T2 H1′−LU H4; H, A5 H1′−LU H7; and I, A5 H1′−LU H6.

connecting these proton pairs (Figure 4). Note that the exchange process takes place between two *bound* and *symmetrical* conformations of the naphthalimide rings (see below), so that only six drug aromatic proton resonances are observed in the D6−LU complex (Figure 2), as would also be the case in the absence of exchange. In contrast to

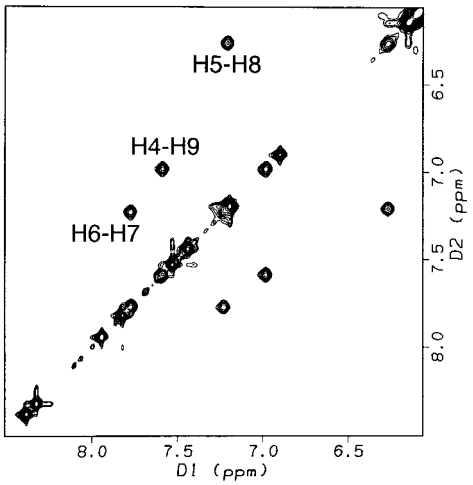

FIGURE 4: Aromatic region of the 500 MHz pure chemical exchange spectrum (mixing time 50 ms) of D6−LU in ^2H_2O at 2 °C, showing the cross-peaks between symmetrical and exchanging naphthalimide protons. No exchange cross-peaks are detected between the LU aminoalkyl linker protons.

the aromatic protons, no exchange cross-peaks are observed for the aminoalkyl linker protons of the drug in the D6−LU complex (not shown).

For convenience, we will designate the LU aromatic H4, H5, H6, H7, H8, and H9 resonances as protons (Figure 1a). Strictly speaking, however, any given LU aromatic proton resonates at each of two exchanging chemical shifts 50% of the time. At 2 °C, the exchange rate between the two ring conformations is more rapid than the interproton dipolar relaxation rate (see below) and affects the NOEs between DNA protons and LU naphthalimide protons. However, the naphthalimide resonances and their NOE interactions could still be unambiguously assigned by performing several NOESY experiments involving selective irradiation of one of the LU aromatic resonances during the mixing time (*14, 32*). In this way, intermolecular NOEs mediated by chemical exchange could be identified (they are marked with asterisks in Figure 3) and excluded from the analyses.

Using this methodology, we determined that one of the central naphthalimide protons (labeled H8) is located near the DNA C4 H2′/H2″ protons (peak B in Figure 3) and also interacts with C4 H6 and A5 H8 (not shown). One of its vicinal protons (H7) gives rise to NOEs with the H1′ (peak H), H4′, and H5′/H5″ protons of A5, while the other vicinal proton (H9) interacts primarily with C4 H5 (peak F) and C4 H6 (not shown). These NOE interactions indicate that this naphthalene half of the drug is situated between the C4 and A5 bases and that the H7 and H9 resonances correspond to its "internal" and "external" positions, respectively (Figure 9). The other central naphthalimide proton (H5) is overlapped with LU H7 (Figure 2) and interacts primarily with A5 H2. One of its two vicinal protons (H6) shows NOE interactions with A5 H1′ (peak I, partly mediated by H7 exchange) and with A5 H2; the other vicinal proton (H4) is close to the T2 sugar protons H1′ (peak G), H2′, and H2″ (peaks C) and also gives rise to a weaker NOE with G3 H8. This indicates that this naphthalene half of the drug is located between T2 and G3 and that H6 and H4 correspond to its internal and external positions, respectively (Figure 9). The NOE interactions of the aromatic LU protons with the H1′ protons of T2 and A5 and with the H2′ and H2″ protons of T2 and C4 further confirm that intercalation takes place between T2 and G3 and between C4 and A5 (Figures 1b, 6, and 9), as indicated by the weakened sugar−base sequential connectivities observed for these steps (Figure 3). Furthermore, the NOE interactions of aromatic LU protons with T2 H1′, A5 H1′, and A5 H2 indicate that the hydrogen-rich naphthalene edge of the naphthalimide system protrudes into the minor groove of D6. The imide-containing edge, and therefore the aminoalkyl linker, must then be located in the major groove of the DNA molecule.

Corroborative evidence for LU binding to the major groove of D6 is provided by the strong NOEs between the C4 HN4 amino protons and the H5′1/2 protons of the LU aminoalkyl linker (pair of peaks A in Figure 3a) and by strong NOEs between the methyl protons of T2 and the H1′1 and H1′2 LU linker protons (not shown). Aminoalkyl linker protons H2′1 and H2′2 also give rise to NOEs with the T2 methyl, C4 amino (peaks E), and G3 H8 protons. Linker protons H4′1 and H4′2 give rise to weak NOE interactions with C4 amino protons (peaks D) and to weaker interactions with the T2 methyl groups. The high intensity of the C4 HN4−LU H5′1/2 NOEs (peaks A) indicates that the central H5′1/2 methylene group of the LU linker is oriented toward the DNA molecule. The relatively strong NOEs between T2 Me and the linker protons H2′1 and H2′2, together with the weak NOE interactions detected between the H2′1 and H2′2 and the H5′1/2 LU linker protons, leaves the H2′1,2 methylene groups facing the solvent and therefore indicates that the protonated amino groups of the drug must be oriented toward the DNA major groove.

Average Structure Determination and Overview. By use of distance and dihedral constraints obtained from the above analyses, 15 structures were independently generated by distance geometry and refined by NOESY back-calculation and r-MD in vacuum. The final refined structures converged to a pairwise rms difference of 0.53 ± 0.20 Å (Figure 5a), an average R_{NOE} factor of 0.31 ± 0.005, and very low constraint violation energies (Table 1).

Figure 6 shows a stereoview of one of the refined D6−LU structures, which represent the average of the two equivalent exchange conformations of the stacked naphthalimide rings. The two naphthalimide rings of the drug are bisintercalated at positions T2pG3 and C4pA5, and the aminoalkyl linker lies in the major groove of the DNA molecule. The drug chromophores stack diagonally with respect to the DNA base pairs, essentially overlapping with the purine bases G3 and A5 from opposite strands (Figure 9). In accordance with the NOE interactions described above, the naphthalene side of the rings protrudes into the minor groove near the sugar protons of T2, C4, and A5, whereas the imide edge is located below the methyl group of T2.

The DNA protons most shifted by LU binding, i.e., G3 HN1, C4 HN4 (internal), A5 H2, and T2 HN3 (Figure 2), are consistently those closest to the naphthalimide chromophores (Figure 9). The same is true for the LU aromatic protons H8 and H4, which are the only drug protons directly above or below the DNA bases. LU H8 is strongly shifted upfield because it is sandwiched between the ring currents of the A5 and C4 bases, whereas LU H4, which is also shifted upfield, is directly above the imidazole ring of G3 (Figure 9).

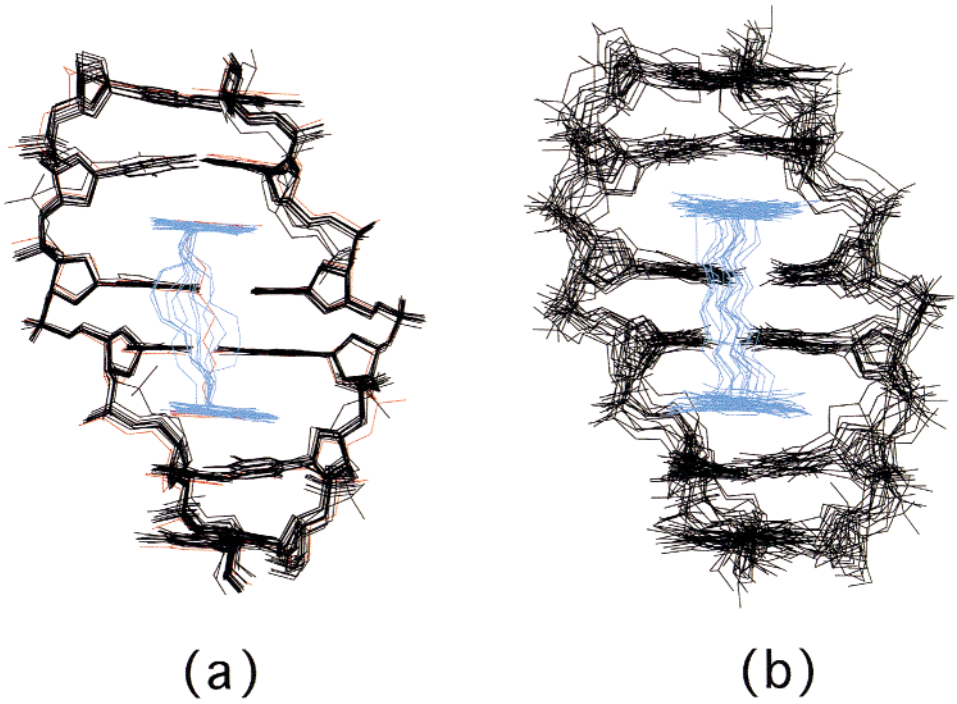

FIGURE 5: (a) Superimposed 15 final refined structures of the D6−LU complex. (b) Fifteen superimposed structures collected at regular intervals during the solvated tar-MD simulation. D6 and LU are colored black and blue, respectively. In panel a, the energy-minimized D6−LU structure averaged over the 400 ps tar-MD trajectory is shown in red and superimposed with the back-calculated structures.

Table 1: Structural and Energy Data for the 15 Refined D6−LU Structures

total potential energy[a] (kcal mol^{-1})	−117.6 ± 6.8
distance restraint violation energy[b] (kcal mol^{-1})	5.2 ± 0.4
dihedral restraint violation energy[c] (kcal mol^{-1})	0.3 ± 0.5
total number of distance restraints	296
intraresidue (D6)	111
intraresidue (LU)	1
interresidue (D6)	128
intermolecular (D6−LU)	42
hydrogen-bonding (D6)	14
total number of dihedral restraints	88
backbone (D6)	52
chiral (D6)	36
number of distance violations > 0.20 (Å)	0
maximum distance violation (Å)	0.15 ± 0.00
rms deviation from ideal bond lengths (Å × 10^2)	0.65 ± 0.01
rms deviation from ideal bond angles (deg)	1.83 ± 0.07
pairwise rms difference[d] (Å)	0.53 ± 0.20
NOE *R* factor[e]	0.31 ± 0.01

[a] Does not include restraint terms; force field parameters specified in Materials and Methods. [b] $K = 30.0$ kcal mol^{-1} Å^{-2}. [c] $K = 90.0$ kcal mol^{-1} rad^{-2}. [d] Calculated excluding hydrogen atoms. [e] Calculated from 232 NOE intensities with a tumbling time of 2.5 ns.

In all the refined structures, one of the protonated amino groups of the LU aminoalkyl linker is hydrogen-bonded to O6 of guanine in the major groove. The other one is either hydrogen-bonded to guanine O6 of the opposite strand or else establishes a weaker hydrogen bond with N7 of the same base. Within this common scheme, the conformation of the LU aminoalkyl linker in the refined structures is variable (Figure 5a), and there are five different linker conformations or hypercubes among the 15 refined structures. The flexibility of the LU aminoalkyl linker will be further investigated in the next sections.

Internal Motion of LU in the D6−LU Complex. Using 2D NOESY, ROESY and pure chemical exchange (*15*) experiments, we established above that an exchange process involving naphthalimide ring rotation takes place between two stacked and symmetrical conformations of the LU chromophores. At 2 °C, the flipping rate is slow on the chemical shift time scale (20 s^{-1}), thus permitting the determination of the structure of the D6−LU complex. As the temperature is increased, the resonances of the LU naphthalimide ring protons progressively broaden and coalesce. At 36 °C the exchange rate becomes intermediate to fast on the chemical shift time scale (1800 s^{-1}), so that only three LU aromatic resonances are observed at the H4−H9, H5−H8, and H6−H7 average chemical shifts (Figure 7). The activation energy for the LU two-ring flipping process, derived from the temperature dependence of the exchange rate (Figure 8), is 21.6 kcal mol^{-1}.

Note that the LU rings rotate by 180° between two symmetric *intercalated* states, so that most of the time they remain stacked into the DNA duplex, even at higher temperatures. This is indicated by the unchanging DNA chemical shifts, which remain constant at their complexed state values when the LU aromatic lines are broadened and coalesced by exchange (Figures 2 and7).

In contrast to the aromatic protons of the drug, the hydrogens of the LU aminoalkyl linker are *not* affected by the above conformational exchange and remain in a unique chemical shift environment bound to the DNA major groove. No exchange cross-peaks are detected between these protons, and their line widths remain relatively unaffected over a broad range of temperatures (Figures 2 and 7). The 15 refined structures depicted in Figure 5a suggest that the aminoalkyl linker region of the drug may be flexible. We have investigated the dynamics of the LU linker on a much shorter time scale (picoseconds to nanoseconds) by measuring the dipolar cross-relaxation rates corresponding to several fixed-distance interproton vectors in the D6−LU complex and

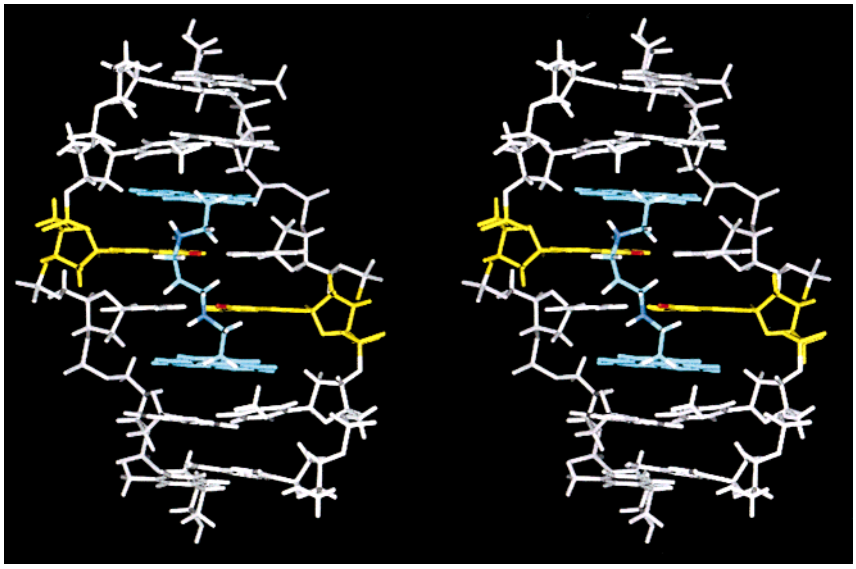

FIGURE 6: Stereoview, toward the major groove, of one of the refined structures of the D6−LU complex. The LU molecule is colored blue, and the guanine nucleotides (with red O6 atoms) are shown in yellow.

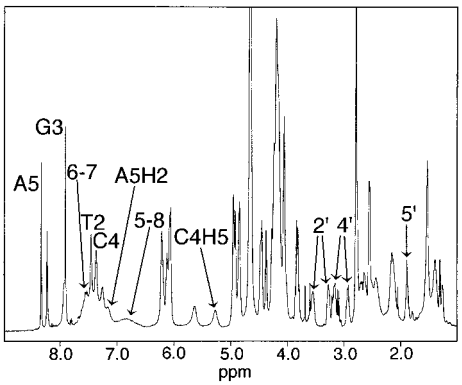

FIGURE 7: ^1H spectra of the D6−LU complex in ^2H_2O at 36 °C. For clarity, only the nonterminal aromatic D6 assignments and the LU assignments (atom numbers) are labeled over the resonances. At this temperature, the LU ring flipping rate is intermediate to fast, and three broad peaks with average chemical shifts corresponding to the exchanging naphthalimide resonance pairs are observed. In contrast, the LU aminoalkyl proton resonances remain relatively unaffected. The LU aromatic 4−9 and linker 1′ lines are overlapped with DNA peaks.

applying the model-free formalism of Lipari and Szabo (*20*). At 2 °C, the order parameters for the LU linker methylene proton pairs are moderately smaller than the order parameter for the reference C4 H5−H6 pair, and decrease progressively toward the center of the linker (Table 2).

Molecular Dynamics with Time-Averaged Restraints. The conformational flexibility of the D6−LU complex was further explored by means of a 400 ps molecular dynamics simulation with time-averaged constraints (tar-MD) (*28*) and explicit solvent. In these simulations, the penalty term for the experimental constraints does not depend on instantaneous violations but on violations averaged over a certain period of time, thus allowing for an increased flexibility of the simulated system. Note that the time scale of this simulation is still 10^6 times shorter than the lifetime of the two LU ring states at 29 °C (1 ms at 1000 s^{-1}), so that we can only study motions occurring on the 0.4 ns and shorter time scale, such as those affecting the cross-relaxation rates of the linker methylene protons.

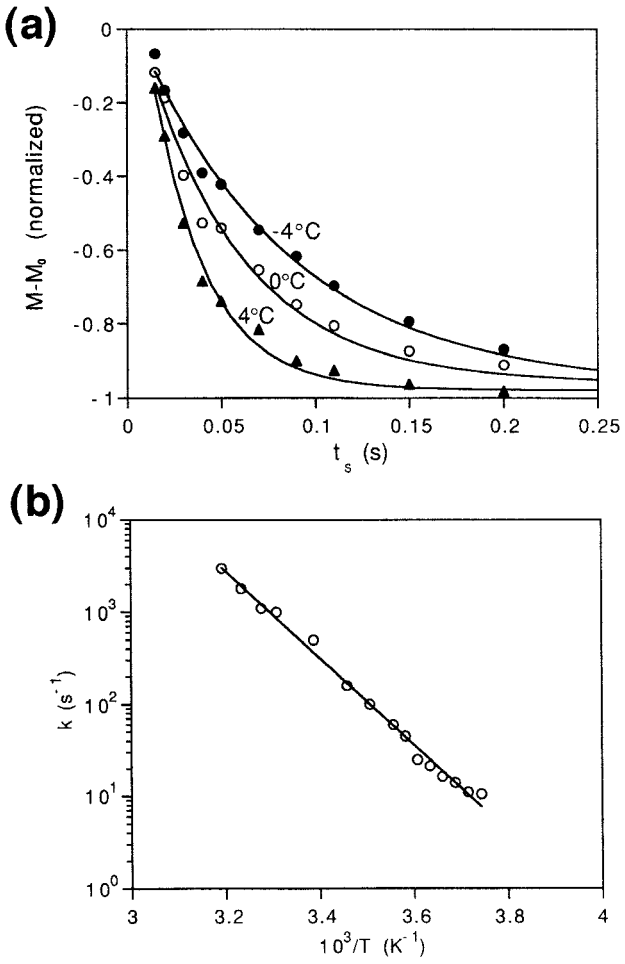

FIGURE 8: (a) Longitudinal magnetization of H9 ($M - M_0$, where M_0 is equilibrium magnetization) as a function of the time during which the H4 exchanging resonance is saturated, at three different temperatures. (b) Naphthalimide ring 180° flipping rate constants (k, per second) as a function of temperature ($1/T$, with T in kelvins) in D6−LU, calculated from saturation transfer experiments ($T < 6$ °C) and bandshape analysis.

Figure 5b shows 15 superimposed D6−LU structures selected at regular intervals during the 400 ps tar-MD simulation, which can be compared with the 15 structures

Table 2: Order Parameters[a] (S^2) for Resolved Proton Pairs with a Fixed Interproton Distance in D6−LU

D6−LU	S^2
C4 H5−H6	1.00
C4 H2′−H2″	0.66 ± 0.07
LU H1′1−H1′2	0.80 ± 0.06
LU H2′1−H2′2	0.65 ± 0.05
LU H4′1−H4′2	0.53 ± 0.01

[a] The C4 H5−H6 pair is used as a reference and assigned $S^2 = 1$. The S^2 values are averaged over two independent series of NOESY intensities (at 25, 50, 100, and 150 and 10, 25, 50, 100, and 150 ms mixing time). For the methylene proton pairs, mixing times below 100 ms were used.

refined in vacuum (Figure 5a). Although the fluctuations are obviously larger, the structure averaged over the 400 ps tar-MD trajectory is quite similar to the back-calculated structures (average rms deviation 0.71 ± 0.09 Å; Figure 5a). In the next sections we will analyze and compare the 15 structures refined in a vacuum, together with a set of 400 structures extracted from the tar-MD trajectory.

DNA Structure. Upon LU binding, the T2:A5 and G3:C4 base pairs are separated, the TpG and CpA steps are unwound, and the minor groove of D6 is widened. We observe 6.5 Å rise values as well as a moderate left-handed unwinding angle of 10° for the T2pG3 and C4pA5 intercalated steps. DNA unwinding is propagated to the terminal base pairs (the total unwinding angle in D6−LU is 47°), but it is difficult to assess whether those angles are significant or affected by end effects. During the tar-MD simulation, a small bending of the D6 helix axis toward the major groove is detected at the terminal steps. The T2:A5 base pair is buckled by 20° in both the back-calculated and tar-MD structures. The central GpC step in the D6−LU complex superimposes particularly well with a standard B-DNA GpC step, indicating that LU-induced DNA deformation is minimal for this central region of the DNA molecule.

Sugar Conformation. In the back-calculated D6−LU structures, the internal purine G3 and A5 sugars adopt S-type conformations (C2′-*endo* and C1′-*exo*, respectively). The pyrimidine sugars T2 and C4 located 3′ to the intercalated drug rings adopt C4′-*exo* and O4′-*endo* conformations, respectively. During the 400 ps tar-MD simulation, G3, C4, and A5 assume a range of conformations approximately centered around the pseudorotation phase angles determined in a vacuum, whereas T2 explores a wider set of conformations. Internal pyrimidine sugars, especially T2, appear to be more flexible than internal purine sugars (Supporting Information). The values observed for the refined structures are in agreement with the observed intensity patterns of the intrasugar COSY and intraresidue NOESY cross-peaks in D6−LU compared to uncomplexed D6, which indicate that the pseudorotation phase angles of the T2 and C4 sugars are changed upon LU complexation. We note, however, that the conformation of the C4 sugar seems to be close to O4′-*endo* in the free D6 duplex (Gallego et al., unpublished results).

Backbone Conformation. The backbone torsion angles of the D6−LU complex are near the α (g^-), β (t), γ (g^+), ϵ (t), and ζ (g^-) domains typical of free B-DNA in both the refined and tar-MD structures (we define g^+, g^-, and t as 60° ± 60°, −60° ± 60°, and 180° ± 60°, respectively). The χ glycosidic torsion angles are in the anti range for all nucleotides, with higher anti values for the nucleotides 3′ to the drug chromophores. The observation of fairly standard backbone angles in the complex is consistent with the small (0.1−0.4 ppm) shifts observed for the ^{31}P signals of D6−LU relative to D6 (*22*) and with the relatively modest unwinding angles measured in the D6−LU structures. The above torsions are also in general agreement with the observation of P−H4′ cross-peaks in the ^{1}H−^{31}P correlation spectra of both D6 and D6−LU (not shown) and are further supported by weak H6/H8/H1′/H2′−H5′/H5″ NOEs and by the observed values of $\sum J_{H4'}$ and $\sum J_{H3'}$ couplings (*23*), which are fairly similar in D6 and D6−LU.

LU-79553 Conformation and Interaction with DNA. In both the refined and tar-MD structures, the LU naphthalimide rings are stacked in a cross-stranded manner on the G3 and A5 purine bases, leaving the pyrimidines T2 and C4 unstacked on both sides (Figure 9). The aminoalkyl linker of LU lies diagonally across the major groove of the DNA molecule, forming a hydrophobic "spine" interconnecting the methyl groups of T2 and T8 (Figure 6). The N3′H_2^+ linker amino groups, which are protonated at neutral pH, are located close to the O6 atoms of the guanine bases, with which they establish favorable electrostatic interactions. During the solvated tar-MD simulation, the N3′ linker aminos formed a weak hydrogen bond with O6 of the nearby guanine in the majority of the 400 structures, with average N3′H−O6 distances of 2.0 ± 0.2 and 2.1 ± 0.4 Å, and average N3′-H−O6 angles of 148.0° ± 15.6° and 146.3° ± 18.6°, respectively.

We have assigned 0, +, and − values to the eight rotatable torsions of the LU aminoalkyl linker (Figure 1a). These values correspond to t, g^+, and g^- angles (defined above), respectively, and each unique eight-value set was defined as a conformational state or hypercube (*33*). For the 400 structures of the solvated tar-MD simulation, the conformational state of the linker changed 32 times, but only five different hypercubes were visited. The most visited hypercube was (+000000−), with 303 occurrences out of 400 structures. All structures retain a rough common scheme of methylene group orientation, i.e., H1′1,2 out, H2′1,2 out, HN3′1,2 in (and hydrogen-bonded), H4′1,2 out and H′51,2 in (where out and in refer to approximate outward or inward orientations with respect to the DNA molecule). This conformational pattern is also observed in the back-calculated structures and is consistent with the intermolecular and intramolecular NOEs described above for the LU aminoalkyl linker. Within this general scheme, some *limited* conformational flexibility involving a few hypercubes is observed in the refined structures (Figure 5a, five hypercubes) and in the solvated trajectory. This agrees with the pattern of order parameters detected for this region of the drug in the D6−LU complex at 2 °C (Table 2) and with the observation of different chemical shifts for the two individual protons of each methylene pair of the LU linker, whose environment is not averaged by fast exchange.

DISCUSSION

In this study we have established that the bisnaphthalimide antitumor agent LU-79553 forms a sequence-specific com-

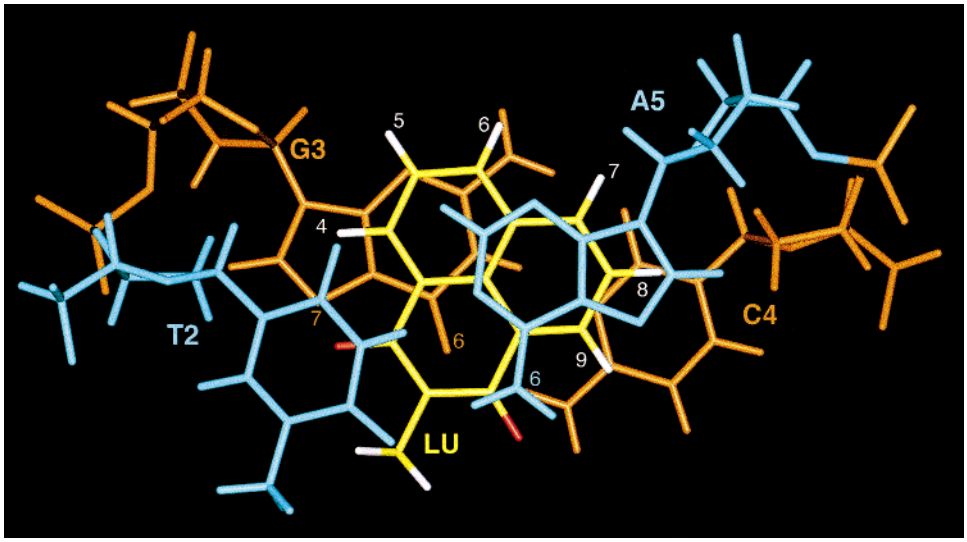

FIGURE 9: Projection down the helix axis of the D6−LU structure, showing the LU naphthalimide ring (in yellow) intercalated between the T2:A5 base pair (blue) and the G3:C4 base pair (orange). The LU oxygens and hydrogens are shown in red and white, respectively, and the naphthalimide hydrogens are labeled. The D6−LU structure corresponds to the restrained energy-minimized average of the 400 tar-MD snapshots.

plex with the hexanucleotide d(ATGCAT)$_2$. The two naphthalimide chromophores bisintercalate at the TpG and CpA steps of the DNA molecule, sandwiching the two central G:C base pairs. The *N*,*N*′-bis(ethylene)-1,3-propylenediamine chain linking the two naphthalimide rings lies in the major groove of the DNA molecule, with its amino groups hydrogen-bonded to the guanine bases.

Our results are in agreement with those of Bailly et al. (*2*), that also concluded bisnaphthalimide binding to the major groove by use of chemical probing. The bisnaphthalimide agents are part of a growing family of intercalating drugs that recognize the major groove of the DNA polymer, such as the bisintercalators ditercalinium (*34*) and flexi-di (*35*).

A surprising result of this study is the observation of exchange between two equivalent intercalated states of the naphthalimide rings in the D6−LU complex. This interconversion process does not involve the aminoalkyl linker of the drug, i.e. the linker linewidths and linker−DNA NOEs are relatively invariant over a broad range of temperatures (Figures 2 and 7), and no exchange cross-peaks are observed between linker protons. Only the two symmetrical halves of both LU chromophores exchange their stacking environment with the DNA bases. This ring flipping interconversion likely takes place via 180° rotation around the N−C1′ bond of the drug (Figure 1a) and probably implies a transition state with partial distortion of the DNA base pairs. The exchange process takes place at a rate of 1800 s^{-1} at 36 °C (Figure 7) and has an activation energy of 22 kcal mol^{-1} (Figure 8). Preliminary data suggests that ring rotation may take place *inside* the intercalation site, because the exchange rate is slower in a d(AATGCATT)$_2$−LU 1:1 complex (Gallego et al., unpublished results). We stress that this is not an exchange process between bound and unbound states but between two bound drug conformations. Indirect proof of strong binding of LU to D6 comes from the marked stabilization of the hexanucleotide duplex upon LU binding, as evidenced by a 19 °C increase in melting temperature (Gallego et al., unpublished results). Although the rotation of buried aromatic rings is well documented in proteins (e.g., ref *36*), to our knowledge this type of flipping motion is unprecedented for an intercalated system, and its mechanism is being investigated.

In the D6−LU complex, the imide side of the LU naphthalimide chromophores is oriented toward the DNA major groove, and the rings are stacked between the purine G3 and A5 bases from opposite strands. The attached ethylenamino groups of the linker are within hydrogen-bonding distance from O6 of guanine, but this also forces the electronegative imide side of the LU chromophore to stack above the markedly electronegative edge of the guanine base (Figure 9). This unfavorable electrostatic stacking interaction is likely to play a role in the unusual flipping motion observed for the LU rings. In this regard, we note that electrostatic stacking interactions have been shown to determine the conformation of DNA bases in intercalated systems (*37*) and to influence the DNA binding specificity of intercalating drugs (*38*).

Interproton cross-relaxation rates at 2 °C (Table 2) and a tar-MD simulation indicate that there is limited flexibility for the LU aminoalkyl linker region on the picosecond time scale. Intermolecular and intramolecular NOEs as well as different chemical shifts for the protons of each linker methylene pair also indicate that the methylene hydrogens of the linker, although flexible, have relatively fixed orientations in the major groove and that the linker amino groups are hydrogen-bonded to the guanine bases.

The LU rings are accommodated at the intercalated TpG and CpA steps of D6 with only moderate (10°) unwinding angles as well as relatively small changes in the phosphodiester torsions. The structural changes at the central GpC step are minimal; this step is less unwound and superimposes well on a standard B-DNA GpC step. Upon LU binding, the pyrimidine T2 and C4 sugars located 5′ to the LU chromophores adopt C4′-*exo* and O4′-*endo* conformations, respectively, in the refined structures. The approximate N-type and S-type pattern observed for the D6 sugars on the 5′ and 3′ side of the LU rings, respectively, has been reported in other DNA intercalated complexes (e.g., refs *39* and *35*).

However, these changes must be sequence-dependent as well as position-dependent, because in the DNA binding sites of quinoxaline bisintercalators, the pyrimidine sugars 3′ to the inserted chromophores are in N-type instead of S-type conformation in solution (*40*).

The solvated tar-MD trajectory provides a more realistic simulation environment and allows for an increased flexibility of the restrained system, enabling us to analyze the conformational fluctuations of the LU and D6 molecules on the picosecond time scale. For the LU linker, we have concluded that there is limited flexibility involving a few hypercubes. For the DNA deoxyriboses, pyrimidine sugars appear to be more flexible than purine ones, for which smaller fluctuations around the back-calculated conformations are observed. The O4′-*endo* state is significantly populated in C4 and A5, and with the exception of T2, we do not observe large interconversions between C2′-*endo* and C3′-*endo* states.

A DNA deformation observable only during the solvated tar-MD trajectory involves a slight bending of the longitudinal axis of D6 toward the major groove. This deformation is probably induced by the electrostatic asymmetry (*41*) derived from the presence of the two positive charges of the LU aminoalkyl linker in the major groove and has also been observed in MD simulations of ditercalinium and flexi-di bound to DNA (*42*).

Binding Specificity. Although TGCA was reported to be the strongest LU binding site in a plasmid pBS DNA fragment (*2*), the identification of a DNA sequence containing a unique binding site for LU was hampered by binding of the drug to multiple binding sites. A separate study on the DNA binding specificity of LU will be published elsewhere, but some salient points are discussed below.

For LU binding to DNA, the aminoalkyl linker seems to be the main factor governing the groove recognition as well as the binding specificity of the drug. Its two cationic amino groups are close to the markedly electronegative region of the major groove defined by the O6 and N7 atoms of guanine in the GpC binding site and are within hydrogen-bonding distance from guanine O6. In this position, these cationic amine functions are also close to the phosphate groups of guanine due to the natural right-handed twist of the DNA helix (Figure 6), so that additional favorable electrostatic interactions are established when LU binds to GpC from the major groove (Gallego et al., unpublished results). Interestingly, the aminoalkyl linker is located below the methyl groups of thymine, so that a hydrophobic "spine" is created in the major groove of the DNA molecule (Figure 6). This effect may be enhanced in the bisnaphthalimide DMP-840 (bisnafide) (*9, 5*), that contains two extra methyl groups in the 1′ position (Figure 1a) of a similar aminoalkyl linker.

Due to the above driving interactions, the naphthalimide chromophores stack with their electronegative imide edge above the markedly electronegative N7/O6 edge of guanine. As discussed above, this unfavorable interaction may play a role in causing the observed rotational motion of the drug rings and is partly compensated by the presence of the electropositive N6 amino group of adenine on the other side of the intercalation step (Figure 9). This favorable electrostatic stacking interaction may be part of the reason why the drug intercalates specifically at mixed TpG (CpA) steps.

The conformation of the unbound DNA molecule may also play a role in the binding specificity of the bisnaphthalimide agents. We have already discussed the fact that (i) the C4 sugar is probably close to an O4′-*endo* conformation in the free D6 duplex, (ii) pyrimidine sugars tend to adopt non-S-type pseudorotation phase angles more easily than do purine sugars, (iii) that a 5′-N, 3′-S sugar conformation pattern has been frequently observed in drug-intercalated DNA complexes, and (iv) deformation of the central GpC step by LU is minimal. On the other hand, TpG (CpA) steps have been reported to be particularly flexible, containing either a large positive roll angle or poor base stacking (*43, 44*). It is thus possible that the TpG (CpA) steps are more easily converted into a LU-bound conformation than are other DNA dinucleotides and that the drug consequently intercalates into those steps while inducing minimal changes in the more stable GpC step of its preferred TGCA binding site.

Antitumor Activity. LU and other naphthalimide agents interfere with the activity of human topoisomerase II (*1, 3, 8, 9*). Many topoisomerase II-blocking compounds contain a DNA-interacting planar ring and a side chain likely representing enzyme-interacting moieties (*10*). Since a DNA major-groove recognition domain has been identified in yeast topoisomerase II (*45*), it is possible that the major-groove-binding aminoalkyl linker of LU interferes with the recognition of DNA by the enzyme.

Some of the strongest DNA−drug−enzyme binding sites for the mononaphthalimide amonafide contain the sequence TGCA (*8*). The DNA binding sequence for LU in the present study is TGCA, and this sequence was also reported to have the best footprint upon binding of LU to pBS plasmid DNA (*2*). From these results, it seems that the requirements for mononaphthalimide−DNA−topoisomerase ternary complex formation are similar to those necessary for specific LU intercalation into DNA. This could contribute to explain the high antitumor activity of the bisnaphthalimide derivatives, as suggested by Bailly et al. (*2*). The composition of the base pairs flanking the bisintercalation site is determined in part by stacking interactions with the drug chromophores, which can in this way modulate the site selectivity of topoisomerase II blocking.

We have characterized a rotational motion of the naphthalimide chromophores in the $d(ATGCAT)_2$−LU complex and have also detected a marked stabilization of the DNA duplex upon LU binding. It has been proposed that base binding pockets are present in the active site of topoisomerase and that enzyme-blocking drugs could compete with unpaired DNA bases for binding to these sites (*46, 10*). Hypothetically, the same forces that cause LU ring flipping in its intercalation site may facilitate the extrusion of the drug rings from the DNA helix and their binding to a hydrophobic pocket in the enzyme, enhancing in this way the blocking of topoisomerase II function.

ACKNOWLEDGMENT

We thank Knoll AG and Dr. Federico Gago for kindly providing us with LU-79553. We also thank Elisabeth B. Golden for excellent technical assistance with DNA purification, Dr. F. Gago for useful discussions, Dr. Tom Pratum for help with the implementation of Bruker software, and Dr. Alex D. Bain for providing the lineshape analysis program MEXICO.

SUPPORTING INFORMATION AVAILABLE

One table with the chemical shifts of D6, LU, and D6−LU and five figures showing the 1D ^{1}H NMR spectra of D6 (2 °C) and D6−LU (16 °C), selected structural parameters for D6−LU, a distribution analysis of sugar pseudorotation angles in D6−LU, the H1′/H3′−H2′/H2″ region of the DQF−COSY spectrum of D6−LU, and the ^{1}H−^{31}P correlation spectrum of D6−LU. This material is available free of charge via the Internet at http://pubs.acs.org.

REFERENCES

1. Bousquet, P. F., Braña, M. F., Conlon, D., Fitzgerald, K. M., Perron, D., Cocchiaro, C., Miller, R., Morán, M., George, J., Qian, X.-D., Keilhauer, G., and Romerdahl, C. A. (1995) *Cancer Res. 55*, 1176−1180.
2. Bailly, C., Braña, M. F., and Waring, M. J. (1996) *Eur. J. Biochem. 240*, 195−208.
3. Braña, M. F., Castellano, J. M., Morán, M., Pérez de Vega, M. J., Romerdahl, C. R., Qian, X.-D., Bousquet, P., Emling, F., Schlick, E., and Keilhauer, G. (1993) *Anticancer Drug Des. 8*, 257−268.
4. Braña, M. F., Castellano, J. M., Morán, M., Pérez de Vega, M. J., Perron, D., Conlon, D., Bousquet, P. F., Romerdahl, C. A., and Robinson, S. P. (1996) *Anticancer Drug Des. 11*, 297−309.
5. Thompson, J., Pratt, C. B., Stewart, C. F., Bowman, L., Zamboni, W. C., and Pappo, A. (1998) *Invest. New Drugs 16*, 45−49.
6. Gupta, R., Liu, J., Xie, G., and Lown, J. W. (1996) *Anticancer Drug Des. 11*, 581−596.
7. Lokey, R. S., Kwok, Y., Guelev, V., Pursell, C. J., Hurley, L. H., and Iverson, B. L. (1997) *J. Am. Chem. Soc. 119*, 7202−7210.
8. De Isabella, P., Zunino, F., and Capranico, G. (1995) *Nucleic Acids Res. 23*, 223−229.
9. Nitiss, J. L., Zhou, J., Rose, A., Hsiung, Y., Gale, K. C., and Osheroff, N. (1997) *Biochemistry 37*, 3078−3085.
10. Capranico, G., Binaschi, M., Borgnetto, M. E., Zunino, F., and Palumbo, M. (1998) *Trends Pharm. Sci. 18*, 323−329.
11. Gallego, J., Golden, E. B., Stanley, D. E., and Reid, B. R. (1999) *J. Mol. Biol. 285*, 1039−1052.
12. Fasman, G. D., Ed. (1975) *Handbook of Biochemistry and Molecular Biology*, 3rd Ed., Part B, Vol. I, p 589, CRC Press, Cleveland, OH.
13. Sklenár, V., Piotto, M., Leppik, R., and Saudek, V. (1993) *J. Magn. Reson., Ser. A 102*, 241−245.
14. Massefski, W. Jr., and Redfield, A. G. (1988) *J. Magn. Reson. 78*, 150−155.
15. Fezjo, J., Westler, W. M., Macura, S., and Markley, J. L. (1991) *J. Magn. Reson. 92*, 20−29.
16. Sklenár, V., Miyashiro, H., Zon, G., Miles, H. T., and Bax, A. (1986) *FEBS Lett. 208*, 94−98.
17. Forsén, S., and Hoffman, R. A. (1963) *J. Chem. Phys. 39*, 2892−2901.
18. Jeener, J., Meier, B. H., Bachmann, P., and Ernst, R. R. (1990) *J. Chem. Phys. 71*, 4646−4553.
19. Bain, A. D., and Duns, G. J. (1995) *J. Magn. Reson., Ser. A 112*, 258−260.
20. Lipari, G., and Szabo, A. (1982) *J. Am. Chem. Soc. 104*, 4546−4559.
21. Macura, S., Farmer, B. T., III, and Brown, L. R. (1986) *J. Magn. Reson. 70*, 493−499.
22. Gorenstein, D. G., Ed. (1984) *Phosphorus-31 NMR: principles and applications*, Academic Press, Orlando, FL.
23. Kim, S.-G., Lin, L.-J., and Reid, B. R. (1992) *Biochemistry 31*, 3564−3574.
24. Weiner, S. J., Kollman, P. A., Nguyen, D. T., and Case, D. A. (1986) *J. Comput. Chem. 7*, 230−252.
25. Case, D. A., (1997) AMBER 5.0, University of California, San Francisco, CA.
26. Zhu, L., and Reid, B. R. (1995) *J. Magn. Reson., Ser. B. 106*, 227−235.
27. Cornell, W. D., Cieplak, P., Bayly, C. I., Gould, I. R., Merz, K. M., Ferguson, D. M., Spellmeyer, D. C., Fox, T., Caldwell, J. W., and Kollman, P. A. (1995) *J. Am. Chem. Soc. 117*, 5179−5197.
28. Torda, A. E., Scheek, R. M., and van Gunsteren, W. F. (1990) *J. Mol. Biol. 214*, 223−235.
29. Darden, T., York, D., and Pedersen, L. (1993) *J. Chem. Phys. 98*, 10089−10092.
30. Dickerson, R. E. (1992) NEWHELIX, University of California, Los Angeles, CA.
31. Babcock, M. S., Pednault, E. P. D., and Olson, W. K. (1993) *J. Biomol. Struct. Dyn. 11*, 597−628.
32. Fezjo, J., Westler, W. M., Macura, S., and Markley, J. L. (1991) *J. Magn. Reson. 92*, 195−202.
33. Bruccoleri, R. E., and Karplus, M. (1990) *Biopolymers 29*, 1847−1862.
34. Delbarre. A., Delepierre, M., Garbay, C., Igolen, J., Le Pecq, J.-B., and Roques, B. P. (1987) *Proc. Natl. Acad. Sci. U.S.A. 84*, 2155−2159.
35. Peek, M. E., Lipscomb, L. A., Bertrand, J. A., Gao, Q., Roques, B. P., Garbay-Jaureguiberry, C., and Williams, L. D. (1994) *Biochemistry 33*, 3794−3800.
36. Wüthrich, K. (1981) *Biochem. Soc. Symp. 46*, 17−37.
37. Gallego, J., Luque, F. J., Orozco, M., and Gago, F. (1994) *J. Biomol. Struct. Dyn. 12*, 111−129.
38. Gallego, J., Ortiz, A. R., de Pascual-Teresa, B., and Gago, F. (1997) *J. Comput. Aided Mol. Des. 11*, 114−128.
39. Berman, H. M., and Young, P. R. (1981) *Annu. Rev. Biophys. Bioeng. 10*, 87−114.
40. Gao, X., and Patel, D. J. (1988) *Biochemistry 27*, 1744−1751.
41. Strauss, J. K., and Maher, L. J., III, (1994) *Science 266*, 1829−1834.
42. Pascual-Teresa, B., Gallego, J., Ortiz, A. R., and Gago, F. (1996) *J. Med. Chem. 39*, 4810−4824.
43. Gorin, A. A., Zhurkin, V. B., and Olson, W. K. (1995) *J. Mol. Biol. 247*, 34−48.
44. Dornberger, U., Flemming, J., and Fritzsche, H. (1998) *J. Mol. Biol. 284*, 1453−1463.
45. Berger, J. M., Gamblin, S. J., Harrison, S. C., and Wang, J. C. (1996) *Science 379*, 225−232.
46. Filipski, J. (1983) *FEBS Lett. 159*, 6−12.

BI9915869